Letters in Applied NanoBioScience
Open-Access Journal (ISSN: 2284-6808)

Article
Volume 13, Issue 2, 2024, 77
https://doi.org/10.33263/LIANBS132.077

Role of NanoBioSensor of Gallium Phosphide Sheet for Detecting and Removing of Nitric Oxide & Nitrogen Dioxide: Chemisorption Study by DFT Method

Fatemeh Mollaamin [1,*], Majid Monajjemi [2]

[1] Department of Biomedical Engineering, Faculty of Engineering and Architecture, Kastamonu University, Kastamonu, Turkey
[2] Department of Chemical Engineering, Central Tehran Branch, Islamic Azad University, Tehran, Iran
* Correspondence: smollaamin@gmail.com (F.M.);

Scopus Author ID 35848813100
Received: 15.04.2023; Accepted: 28.05.2023; Published: 30.06.2024

Abstract: The role of the gallium phosphide nanosheet for the adsorption of pollutant gases of nitric oxide and nitrogen dioxide was investigated by applying density functional theory. The fluctuations of charge distributions have demonstrated a more significant charge transfer between graphitic-like gallium phosphide surface (electron acceptor) and gas molecules (electron donors) through the adsorption process. The partial electron density states related to this have illustrated that the nitric oxide and nitrogen dioxide states in the gallium phosphide nanosheet have more of the conduction band, while the developed contribution of P states are near Ga states, but N and O states have minor contributions. Gallium phosphide nanosurface has indicated enough capability for trapping nitric oxide and nitrogen dioxide through charge transfer from N and O atoms to the Ga atoms due to intra-atomic and interatomic interactions.

Keywords: Eco-friendly method; nanoscience; toxic gas scavenging; adsorption system.

1. Introduction

Generally, gas sensors are largely approved with properties such as high selectivity and sensitivity, low cost, small size, long working life, and resistant activity in different environmental statuses [1-5].

Based on the application of graphene as a gas sensor in some works [6-10], it has been confirmed that the charge transfer diffused by adsorbing of gas molecules on the graphene surface might be considered to produce sensitive detectors. Moreover, sensor attributes can change the resistance of the graphene nanosheet once the gas molecules act like acceptors or donors of electrons [11-17].

Thus, making high-implement gas detectors for distinguishing hazardous gases is essential [18-24]. The gas sensors containing metal oxides have been used to recognize hazardous pollutant gases, which have most gas sensing characteristics except accurate selectivity [25]. Their detecting mechanism usually deals with the chemical interaction between the gas molecule and the oxygen molecule adsorbed on the surface because cross sensitivity among various analyte gas compounds is obvious in a metal oxide-based sensor instrument [26,27]. For example, the reconnaissance of SO_2 and NO_2 molecules is prevented due to cross-interference when diffused in a mixed status from a static origin [28].

Recently, two-dimensional nanomaterials with high surfaces of phosphorene and silicene have been known for efficient gas detection, which can largely transfer the charge density between gas molecules and the substrates [29-34].

Semiconductor materials are mainly prepared from the elements in groups II to VI of the periodic table [35]. In the compound in group III-V, each atom of group III is bonded to four atoms of group V for attaining an octet in the valence band when the valence charge from an atom of group V transfers toward an atom of group III and cultivates partial ionic bonding to the crystal surface [36].

The GaN structure is one of the most discovered group III-nitride semiconductors, and it has been applied in different applications, such as electronic and optoelectronic devices and sensor instruments [37-40]. Considering the prominent electronic properties of gallium nitride (GaN), it can be an appropriate case for gas sensing [41-47]. For instance, some studies have exhibited that $Ga_{12}N_{12}$ nanoclusters can gas sense CO, NO, NO_2, and HCN gas molecules [48-51].

Moreover, GaN nanostructures suggest firm action under different radiation and space conditions at room temperature and wide varieties of temperature and humidity compared to metal-oxides [52]. In addition, it has been investigated that magnetic properties, instead of electrical properties owing to the interaction between the gas molecule and surface in the active compound, the PL-GaN sheet could be applied as a largely selective magnetic gas detector for NO and NO_2 sensing [46,47]. DFT computations have been accomplished, and it has been indicated that GaN wurtzoids, as agents of GaN nanocrystals, are appropriate for hydrogen-detecting nanostructures. The nitrogen sites were discovered to have a function for the hydrogen sensing susceptibility. It's obvious that wurtzoids are bundles of capped (3, 0) nanotubes that build the wurtzite phase when they attain nanocrystal or bulk sizes [53].

Moreover, GaP has been investigated as a sensitive material for constructing anodically bonded cells for atomic detectors because its properties containing optical transparency in the near "IR" and high thermal conductivity make it a notable option in sensor devices [54].

One-dimensional semiconductor nanowires often consist of polytypic structures due to the coexistence of various crystal GaAs as semiconductors using the chemical vapor transport approach [55]. The damaging impact of NO_2 on human health and the environment has caused NO2 gas sensors and their state-of-the-art characteristics to be studied [56-58].

Ammonia, "NH_3", is an important ingredient of reactive nitrogen, and it has a prevalent harmful impact on health. Nitrogen atoms in NH_3 help to form atmospheric aerosols that remain in the atmosphere for some time [59-61]. Moreover, "NH_3" is crucial in biology, medicine, and environmental controlling equipment. Recently, GaP epitaxial nanowires have been investigated as an efficient adsorption material for NH_3 detection with a simple device [62].

Therefore, this research wants to investigate the adsorption of hazardous gas of NO and NO_2 by using a monolayer graphitic GaP nanosheet with an atomically flat planar honeycomb hexagonal structure as "PL-GaP" [63-66] employing density functional theory (DFT) to discover the adsorbing parameters of the GaP nanosheet.

2. Materials and Methods

In this research, the simulated calculations have been calculated by Gaussian 16, Revision C.01 [67] using the DFT method. The [Perdew–Burke–Ernzerhof] "PBE" functional with high-precision generalized gradient approximation "GGA" has been employed to achieve more authentic results [68]. Every simulated group contains a graphitic-like length of 25 Å with a bond length of 2.28 Å for GaP with a single NO or NO_2 molecule adsorbed onto it (Scheme1).

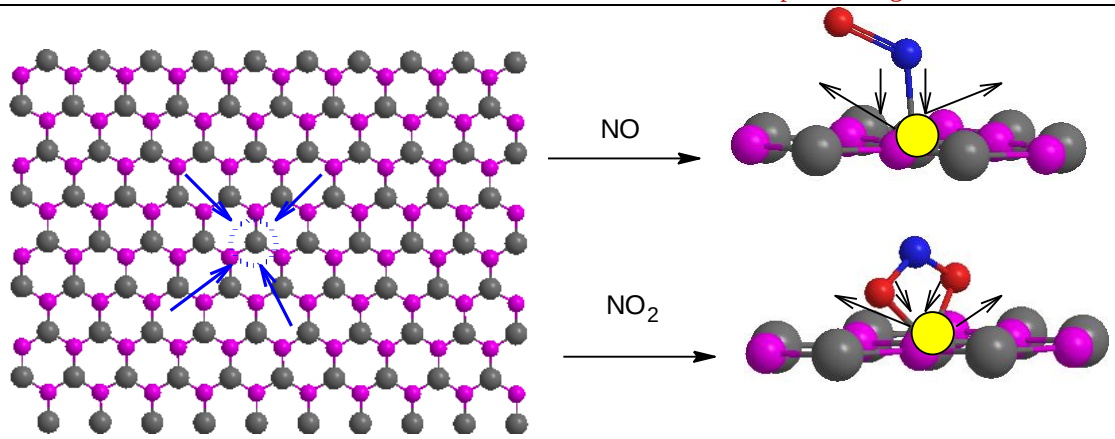

Scheme 1. "Langmuir" adsorption of NO and NO_2 onto GaP nanosheet.

The charge transfer between adsorbates of NO, NO_2, and the adsorbent of GaP nanosheet is calculated using the Bader charge analysis [69]. This method can measure charge accumulation from the charge of each atom in the complex model. Finally, the total adsorption charge transfer can be obtained as a formula: $\Delta Q_t = Q_2 - Q_1$, where Q_2 and Q_1 remark the charge of NO and NO_2 before and after adoption, respectively. As a matter of fact, Positive ΔQ_t indicates that electrons are transferred from gas molecules of NO and NO_2 to the surfaces of the GaP nanosheet, and the adsorbent acts as an electron acceptor [70,71].

The adsorbing of NO and NO_2 gases on the surface of the GaP nanosheet was defined by the theory "Langmuir" isotherm [72-81], which indicates the chemisorption between gas molecules and the GaP surface. The adsorbates of NO and NO_2 molecules are maintained on the surface of GaP with "Langmuir" chemisorption (Scheme1).

The changes of charge density analysis in the adsorption process have illustrated that the GaP nanosheet shows the Bader charge of -0.721e before adsorption of NO & NO_2 and -0.183e, -0.352e, after adsorption of NO & NO_2, respectively.

Therefore, the changes of charge density for "Langmuir" adsorption of NO & NO_2 on GaP surface alternatively are $\Delta Q_{NO \rightarrow GaP} = +0.538 > \Delta Q_{NO2 \rightarrow GaP} = +0.369$.

The total energy of the NO & NO2 molecules and GaP surface should be computed to calculate the adsorption energy. As it has been shown in Scheme 1, we have built a graphitic-like length of 25 Å with a bond length of 2.28 Å for GaP. Then, we tailored the spin-polarized DFT calculation with the "ONIOM" model [82] accompanying the same force and energy convergence accuracy to the adsorption systems, with CAM-B3LYP [83] functional and with 6-311+G (d,p) [84] basis set for nitrogen, oxygen, and LANL2DZ for gallium in the adsorption sites for the first layer (high level). The second layer (medium level) has been considered on some gallium atoms and nitrogen or phosphorus atoms of GaP nanosheet, respectively, in the adsorption site due to semi-empirical methods. The third layer (low level) has been saved on the remaining gallium atoms and also remained nitrogen or phosphorus atoms of GaP nanosheet with molecular mechanic force fields (Scheme 2) [82] as formula: $E_{ONIOM} = E_{1st} + E_{2nd} + E_{3rd}$.

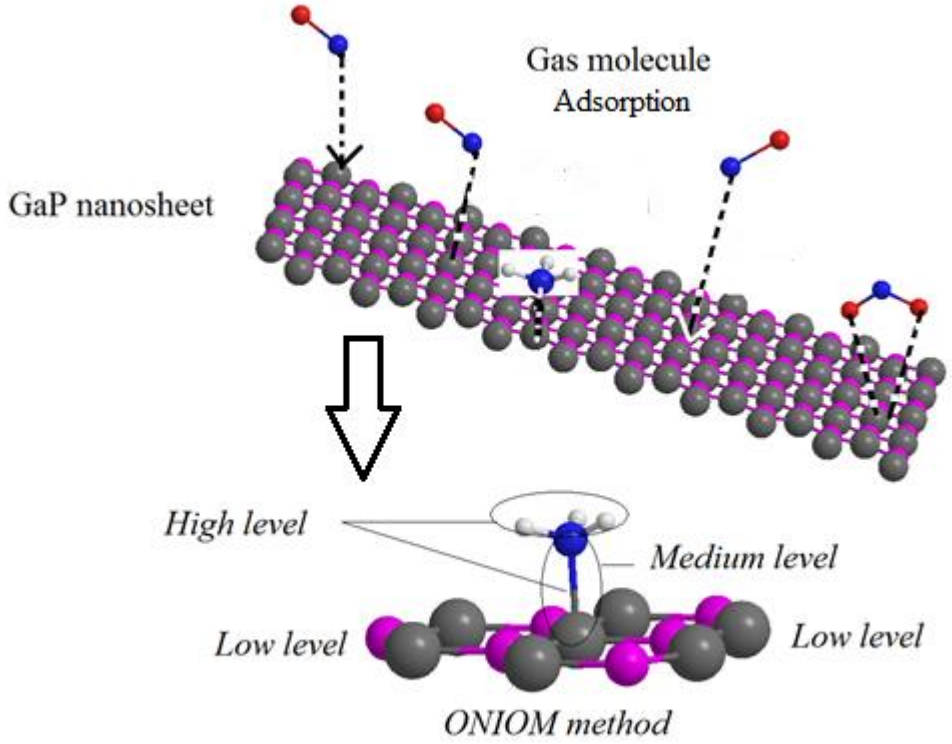

Scheme2. The mechanism of the "Langmuir" adsorption of NO and NO_2, molecules onto GaP nanosheet is based on optimized coordination due to the three-layered high, medium, and low levels of the "ONIOM" method.

The binding energy of each system has been calculated to determine the most sensitive structure of gallium phosphide (GaP) as the selective sensor for detecting gas molecules of NO and NO2. Therefore, we have found that the priority for selecting the surface binding of N-atom of NO and O-atom of NO_2 in the adsorption site can be impacted by the existence of close atoms in the GaP surface. The simulated distribution functions of NO → GaP and NO_2 → GaP have illustrated that the created clusters lead to the bond lengths of N →Ga in NO → GaP (1.44 Å) and O →Ga in NO_2 → GaP (2. 44 Å) (Schemes1 & 2).

3. Results and Discussion

In this verdict, gallium phosphide (GaP) nanosheet has been investigated as the efficient surface because of their structural selectivity for adsorption of nitric oxide (NO) and nitrogen dioxide (NO_2).

3.1. Electronic properties.

The electronic structures of NO and NO_2 adsorbed on the GaP nanosheet have been analyzed to simplify subsequent discussion for interfacial electronic properties using CAM-B3LYP/ LANL2DZ, 6-311+G (d,p) basis sets. The graph of partial DOS (PDOS) has illustrated that the *p* states of N- and O- adsorption on the GaP nanosheet are dominant through the conduction band (Figure 1). A distinct metallic feature can be observed in the GaP nanosheet because of the strong interaction between the *p* states of N, P, and the *d* state of Ga near the Fermi energy. Moreover, the existence of covalent features for these complexes has exhibited the identical energy amount and figure of the PDOS for the *p* orbitals of N, O, P, and *d* orbitals of Ga (Figure 1).

(a)

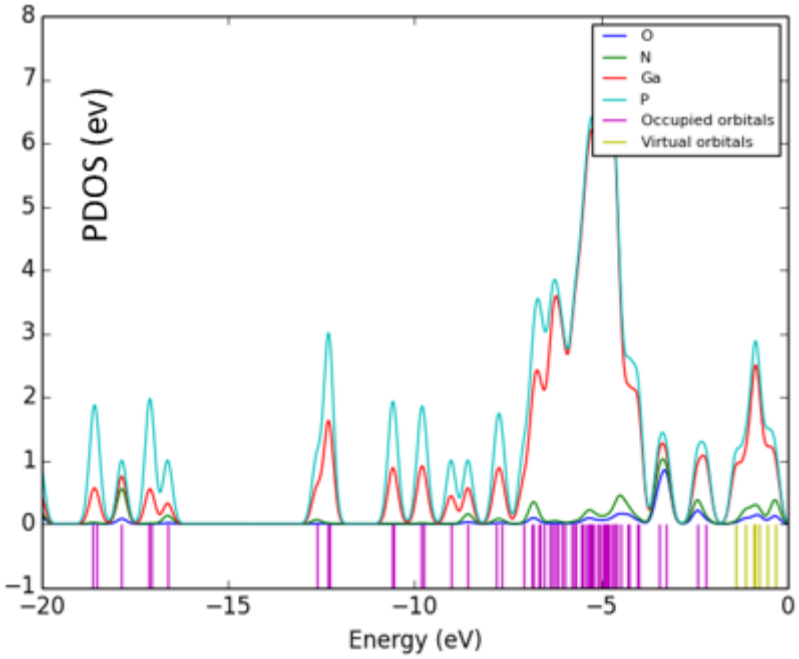

(b)

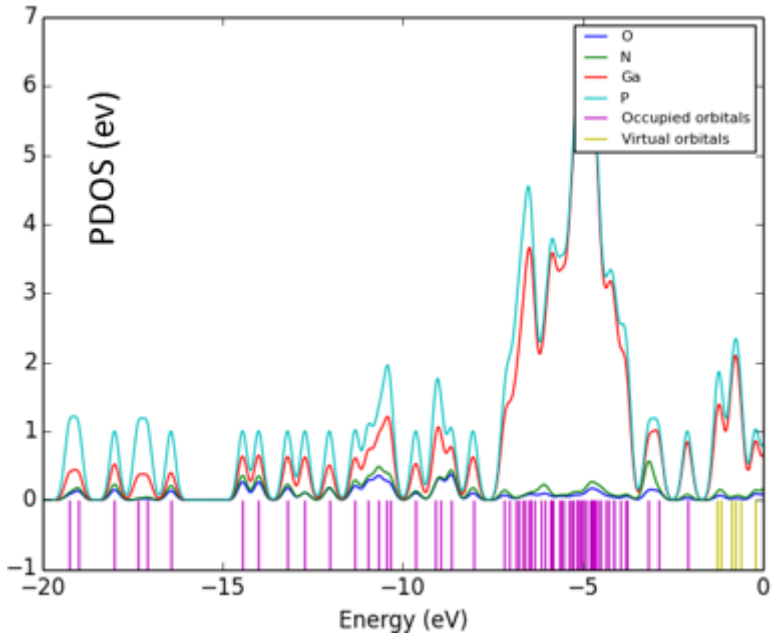

Figure 1. PDOS adsorption of **(a)** NO→ GaP, and **(b)** NO_2→ GaP nanosheets with Fermi level =0.

Figure 1a shows that the NO states in the GaP nanosheet have more contribution at the middle of the conduction band between -5 to -10 eV, while the contribution of gallium and phosphorus sates are expanded and close together, but nitrogen and oxygen states have minor contributions. In addition, Figure 1b illustrates the adsorption of NO_2 onto GaP nanosheet has more contribution at the middle of the conduction band between -5 to -10 eV, while the contribution of gallium and phosphorus sates are expanded and close together, but nitrogen and oxygen states have minor contributions.

The results were also approved by the partial electron density (PDOS), which showed a certain charge association between GaP nanosheet and gas molecules of NO and NO_2.

In other words, the P states in the GaP nanosheet have large contributions in the valence band. Thus, the above results exhibit that the cluster dominant of non-metallic and metallic features and a

certain degree of covalent features can illustrate the increase in the semiconducting direct band gap of gas molecules adsorbing on the GaP nanosheet.

3.2. Nuclear quadrupole resonance (NQR) analysis.

NQR is based on the multipole enlargement in cartesian harmonies as the following equations:

$$V(r) = V(0) + \left[\left(\frac{\partial V}{\partial x_i}\right)\Big|_0 . x_i\right] + \frac{1}{2}\left[\left(\frac{\partial^2 V}{\partial x_i x_j}\right)\Big|_0 . x_i x_j\right] + \cdots \quad (1)$$

Then, after simplification of the equation, there are only the second derivatives dependent on the same variable for the potential energy [85,86]:

$$U = -\frac{1}{2}\int_{\mathcal{D}} d^3 r\, \rho_r \left[\left(\frac{\partial^2 V}{\partial x_i^2}\right)\Big|_0 . x_i^2\right] = -\frac{1}{2}\int_{\mathcal{D}} d^3 r\, \rho_r \left[\left(\frac{\partial E_i}{\partial x_i}\right)\Big|_0 . x_i^2\right]$$

$$= -\frac{1}{2}\left(\frac{\partial E_i}{\partial x_i}\right)\Big|_0 . \int_{\mathcal{D}} d^3 r\, [\rho(r) . x_i^2] \quad (2)$$

There are two parameters that must be obtained from NQR experiments: the quadrupole coupling constant, χ, and the asymmetry parameter of the EFG tensor η:

$$\chi = {e^2 Q q_{zz}}/{h} \quad (3)$$

$$\eta = {q_{xx} - q_{yy}}/{q_{zz}} \quad (4)$$

where q_{ii} are components of the EFG tensor at the quadrupole nucleus determined in the EFG principal axes system, Q is the nuclear quadrupole moment, e is the proton charge, and h is Planck's constant [87].

Since the electric potential for a system of point charges is equal to the sum of the point charges' individual potentials, the calculations are done simply based on the summation of potential fields, which is scalar, instead of the summation of the electric fields, which is vector and much more difficult that potential field. So, $V_E(r) = \frac{1}{4\pi\varepsilon_0} \sum_i \frac{q_i}{|r - r_i|}$, where r is the point at which the potential is measured, r_i is a point at which the charge is ≠0, and q_i is the charge at the point r_i. Finally, the potential of a continuous charge distribution $\rho(r)$ appears: $V_E(r) = \frac{1}{4\pi\varepsilon_0}\int_R \frac{\rho(r')}{|r - r'|} d^3 r'$, where R is a region including all the points at which the charge density is ≠0, r' is a point inside R, and $\rho(r')$ is the charge density at the point r' [88].

NQR method has been carried out for the complexes of NO and NO_2 adsorption on the graphitic-like GaP nanosheet.As the EFG at the position of the nucleus in gas adsorbed on the gallium nitride and gallium phosphide nanosheets as the gas sensor is assigned by the valence electrons twisted in the special linkage with close nuclei of GaP nanosurface, the NQR frequency at which transitions happen is particular for NO→ GaP and NO_2→ GaP clusters (Table 1).

Table 1. The electric potential (E_p) and Bader charge (Q) for elements involved in the adsorption mechanism of NO and NO_2 on the GaP nanosheets using CAM-B3LYP/EPR-III, 6-311+G (d,p) calculation extracted of NQR method.

:Ö = Ṅ:→ GaP			:Ö:−Ṅ = Ö:→ GaP		
Atom	**Q**	**E_p**	**Atom**	**Q**	**E_p**
O1	-0.1121	-22.0983	N1	-0.1672	-18.1325
N2	-0.1830	-18.1953	O2	-0.2476	-21.9465
Ga3	-0.0542	-146.7837	O3	-0.2252	-21.9584
P4	0.0766	-53.3514	Ga4	-0.0473	-146.824
Ga5	-0.0238	-146.8043	P5	0.1540	-53.306
Ga6	-0.0337	-146.7962	Ga6	-0.1367	-146.787
P7	0.0826	-53.4215	Ga7	-0.1310	-146.787
Ga8	-0.0458	-146.7722	P8	0.1304	-53.4033
P9	0.1161	-53.4000	Ga9	-0.0419	-146.777
P10	0.0872	-53.3442	P10	0.0977	-53.4119

:Ö = Ṅ:→ GaP			:Ö:–Ṅ = Ö:→ GaP		
Atom	**Q**	**E_p**	**Atom**	**Q**	**E_p**
Ga11	0.0255	-146.7736	P11	0.0535	-53.3514
Ga12	-0.0543	-146.7907	Ga12	0.3515	-146.765
P13	0.0681	-53.3499	Ga13	-0.0214	-146.816
Ga14	-0.0469	-146.7863	P14	0.1766	-53.2955
P15	0.0977	-53.4117	Ga15	-0.0405	-146.766
			P16	0.0951	-53.4106

In addition, Figure 2 (a,b) plots the electric potential of the NQR method versus Bader charge for elements of nitrogen, phosphorus, oxygen, and gallium in the adsorption process of NO and NO_2 on the GaP nanosheet using CAM-B3LYP/EPR-III, LANL2DZ, 6-311+G (d,p) level of theory.

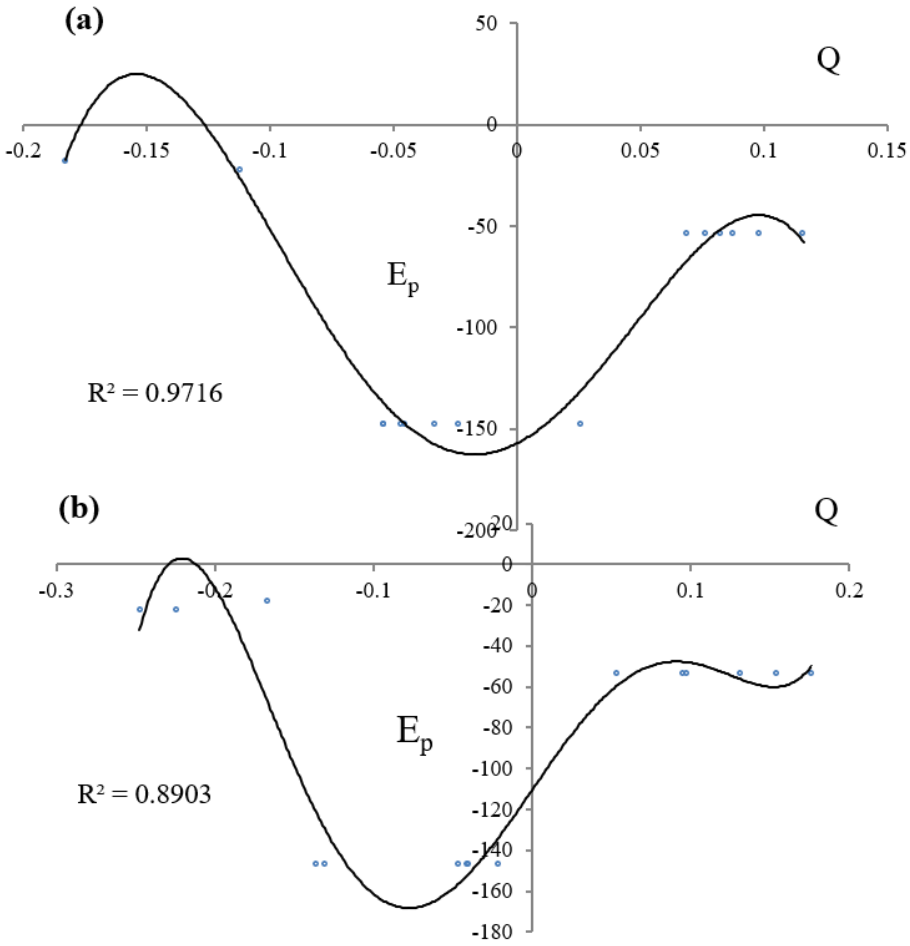

Figure 2. The electric potential versus Bader charge through NQR calculation for adsorption clusters of **(a)** NO →GaP and **(b)** NO_2 →GaP using CAM-B3LYP/EPR-III, LANL2DZ,6-31+G(d,p).

In Figure 2 (a,b), the changes in electric potential for nitrogen, phosphorus, oxygen, and gallium in the active site of Langmuir adsorption have been remarked. In fact, the effect of the binding between N and O with gallium in the GaP nanosheets has been observed during adsorbing NO and NO2 through the resulting electric potential using NQR analysis (Figures 2a and 2b). It's obvious that the capability of GaP for detecting NO and NO_2 fluctuates by their selectivity and sensitivity, which can represent the efficiency of these surfaces as promising sensors.

3.3. "NMR" spectroscopy.

Isotropic (σ_{iso}) and anisotropy (σ_{aniso}) shielding tensors of "NMR" spectroscopy for certain atoms in the active site of NO and NO_2 adsorbed on the GaP nanosheet have been computed applying Gaussian 16, Revision C.01 and reported in Tables2 [67].

Table 2. Data of "NMR" shielding tensors for selected atoms of NO and NO_2 through adsorption on GaP nanosheets using CAM-B3LYP/EPR-III, 6-311+G (d,p) calculation.

$:\ddot{O}=\dot{N}:\rightarrow$ GaP			$:\ddot{O}:-\dot{N}=\ddot{O}:\rightarrow$ GaP		
Atom	**σ_{iso}**	**σ_{aniso}**	**Atom**	**σ_{iso}**	**σ_{aniso}**
O1	4291.3737	18144.2304	N1	963.1386	5073.9512
N2	1501.5049	7351.6689	O2	449.7992	1347.3262
Ga3	11101.4880	32961.8880	O3	240.2882	1770.9646
P4	1345.6299	2994.8451	Ga4	250.7804	17847.5451
Ga5	4597.8176	13217.0292	P5	7.4632	2349.9993
Ga6	8863.2663	27092.9349	Ga6	2265.7391	35940.7712
P7	2450.3875	8540.9915	Ga7	1778.5600	16061.2490
Ga8	10528.6575	42599.5393	P8	1540.9587	6540.2528
P9	2005.8726	12528.0484	Ga9	5545.2324	30081.3134
P10	2001.5489	5508.0432	P10	1832.7918	10443.3200
Ga11	74.6069	7545.0632	P11	1214.9676	2235.8903
Ga12	2070.4614	10425.6100	Ga12	2046.9346	2697.7003
P13	1077.9593	1502.2900	Ga13	280.8469	10404.0217
Ga14	12773.7755	21777.8000	P14	581.4133	946.6701
P15	786.8145	4011.5859	Ga15	12061.3717	22237.3411
			P16	2577.7451	6181.6267

"Isotropic chemical-shielding" (σ_{iso}) & "anisotropic chemical-shielding" (σ_{aniso}) [89] : $\sigma_{iso}=\frac{\sigma 33+\sigma 22+\sigma 11}{3}$; $\sigma_{aniso}=\sigma 33-\frac{\sigma 22+\sigma 11}{2}$

The chemical shielding (ppm) of "NMR" curves versus atom type was observed through adsorption of NO and NO_2 onto GaP nanosheet (Figure 3).

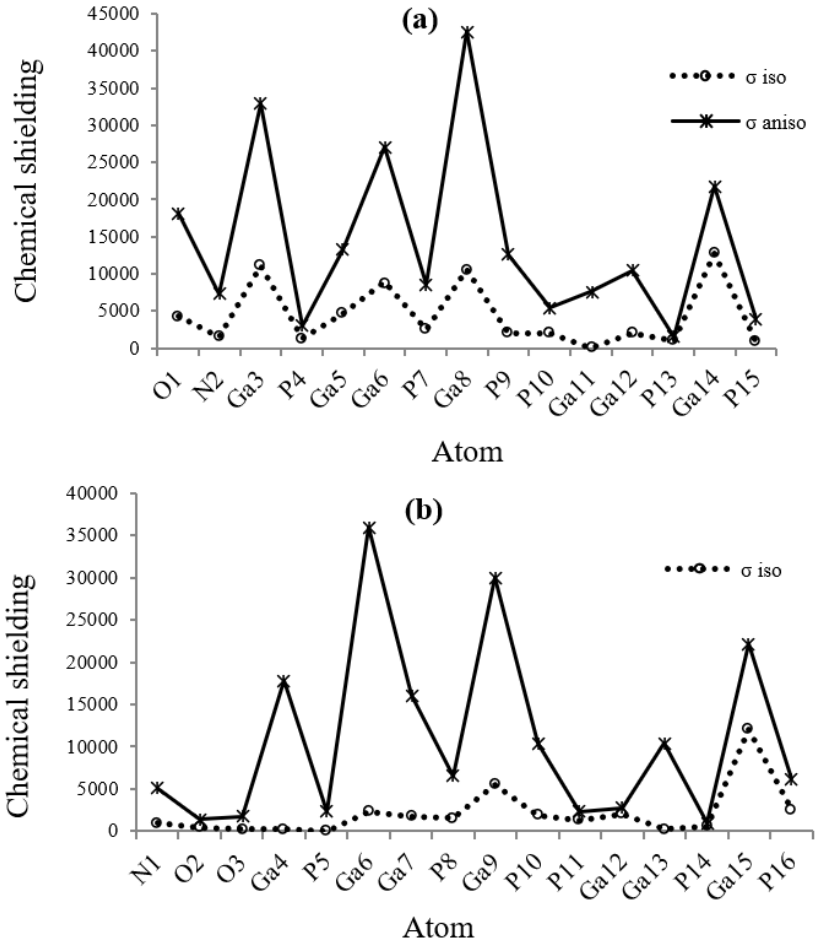

Figure 3. "NMR" adsorbing of NO and NO_2 on the GaP nanosheet through the production of clusters of **(a)** NO→ GaP and **(b)** NO_2→GaP.

The resulting graphs of "NMR" data in Figure3 (a,b) have shown the isotropic and anisotropy factors for NO→ GaP nanosheet with several sharp peaks related to gallium atoms involving the

adsorption site (Ga3, Ga5, Ga6, Ga8, Ga12, Ga14) (Figure3a) and NO_2→ GaP nanosheet with several sharp peaks related to gallium atoms involving the adsorption site (Ga4, Ga6, Ga7, Ga9, Ga13, Ga15) (Figure 3b). Although, in the NMR spectroscopy, the remarkable peak around the gallium atom in the GaP nanosheet has been observed through the adsorption procedure of gas molecules, there are some fluctuations in the chemical shielding behaviors of isotropic and anisotropy attributes.

3.4. "IR" insight & thermodynamic analysis.

In this part, the stability of complexes, including gas adsorption on graphitic gallium phosphide (GaP), has been investigated through thermodynamic properties that define the reactions that gas molecules of nitric oxide (NO) and nitrogen dioxide (NO_2) endure in the gallium coordination sphere. Concerning the adsorption process, the thermodynamic characters were evaluated for NO and NO_2 on the surface of graphitic gallium phosphide (GaP) as the gas detector, which can be applicable as the selective sensor for these gases (Table 3).

Table 3. The thermodynamic character of NO and NO_2 adsorbed on the GaP nanosheet.

Compound	$\Delta E^o \times 10^{-4}$ (kcal/mol)	$\Delta E^o_{ads} \times 10^{-4}$ (kcal/mol)	$\Delta H^o \times 10^{-4}$ (kcal/mol)	$\Delta G^o \times 10^{-4}$ (kcal/mol)	S^o (Cal/K.mol)	Dipole moment (Debye)
Ga-P	-3.2937	-	-3.2936	-3.2964	91.515	0.4347
NO	-8.0017	-	-8.0016	-8.0031	48.968	0.2376
NO_2	-12.6298	-	-12.6298	-12.6315	57.792	0.2323
NO→ GaP	-970.6414	-959.3460	-970.6413	-970.6453	131.438	2.3266
NO_2→ GaP	-975.2858	-959.3623	-975.2858	-975.2897	130.628	2.0852

Furthermore, the "IR" spectrums for the adsorption of NO and NO_2 on the surface of the GaP nanosheet have been reported in Figure 4 (a, b). The graphs of Figure 4a have been observed in the frequency range between 50 cm^{-1}- 500 cm^{-1} for the complex of NO→ GaP with a sharp peak around 200 cm^{-1}.

Figure 4b shows the several strongest IR peaks of NO_2→ GaP clusters, approximately between 200 cm^{-1}- 1150 cm^{-1}. Besides, it has been seen that the frequency sharp peaks of 265 cm^{-1} and 700 cm^{-1} for NO_2→ GaP (Figure 4b).

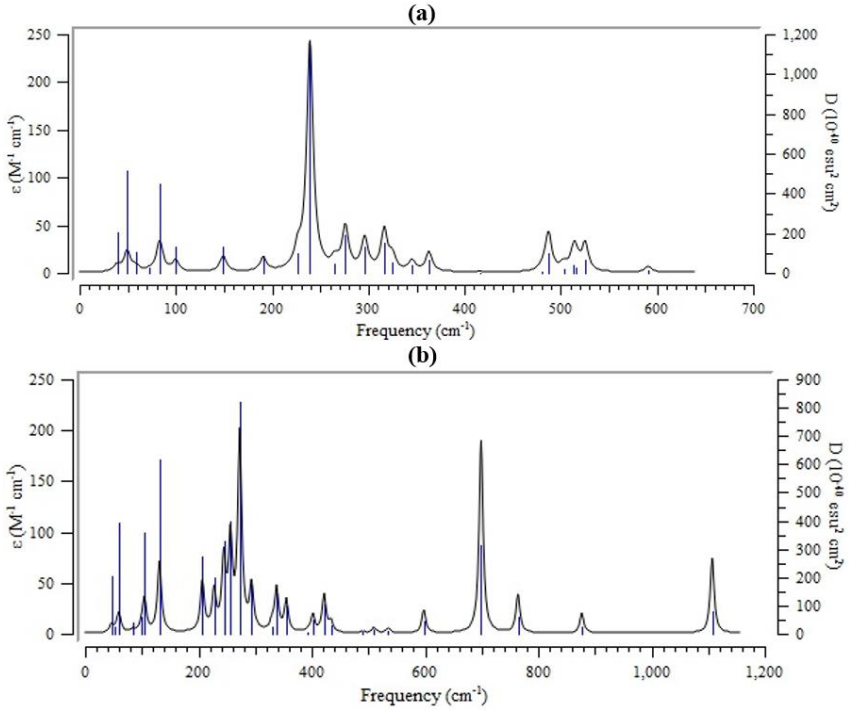

Figure 4. The frequency (cm^{-1}) changes through the "IR" spectrums for **(a)** NO→ GaP and **(b)** NO_2→ GaP nanosheet as the selective gas detector.

The adsorptive capacity of NO and NO_2 on the surface of GaP is approved by the ΔE^o_{ads} amounts as formula:

$$\Delta E^o_{ads} = \Delta E^o_{X\rightarrow GaP} - (\Delta E^o_X + \Delta E^o_{GaP}) \text{ ; } (X=NO \text{ and } NO_2)$$

Table 3 shows that the adsorbing of NO and NO_2 on the surfaces of GaP nanosheet must have both a "physical" and "chemical" nature. All the measured relative adsorption energies (ΔE^o_{ads}) are almost identical and exhibit the accuracy of the calculations and the estimated data by all methods (Table 3).

Furthermore, the results of Table 3 have indicated that NO→ GaP and NO_2→ GaP nanosheets have a large gap of Gibbs free energy adsorption, which defines the changes between Gibbs free energy of initial compounds (ΔG^o_{NO}, ΔG^o_{NO2}) & (ΔG^o_{GaP}) and product compounds ($\Delta G^o_{NO\rightarrow GaP}$, $\Delta G^o_{NO2\rightarrow GaP}$) through polarizability. However, GaP nanosheet seems to possess enough efficiency for adsorbing toxic gases of NO and NO_2.

3.5. Analysis of "HOMO, LUMO".

Based on frontier molecular orbital "FMO" theory, the "LUMO" and "HOMO" and the energy between them is the band gap of the adsorption system was computed. In fact, the broadband gap diagram indicates that there is less conductivity [90-92]. The "LUMO", HOMO", band energy gap (ΔE), and other quantities distributions of NO and NO_2 on the surface of GaP nanosheet as the gas detector system denotes that the gas adsorption procedure scatters the electrons of the system (Table 4).

Table 4. "LUMO" (a.u.), "HOMO" (a.u.), band energy gap (ΔE /eV), and other quantities (eV) distributions of NO and NO_2 adsorbed on the surface of GaP nanosheet.

Gas→ GaP	LUMO	HOMO	ΔE	μ	χ	η	ζ	ψ
NO→GaP	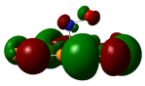 -0.0512	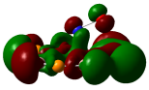 -0.0803	0.7910	-1.7893	1.7893	0.3955	1.2642	4.0475
NO_2→GaP	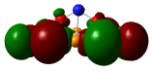 -0.0469	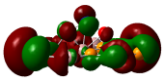 -0.0771	0.8212	-1.6871	1.6871	0.4106	1.2177	3.4660

Band energy gap : $\Delta E = E_{LUMO} - E_{HOMO}$; Chemical potential: $\mu=(E_{HOMO}+E_{LUMO})/2$; Electronegativity: $\chi= -(E_{HOMO}+E_{LUMO})/2$; Hardness :$\eta=(E_{LUMO} - E_{HOMO})/2$; Softness: $\zeta =1/(2\eta)$; electrophilicity index: $\psi = \mu^2/(2\eta)$ [24-26].

The energy gap between HOMO and LUMO has represented the transporting of molecular electrical characters [93]. On the other hand, the difference between HOMO and LUMO has exhibited the effect of the adsorption process on the electronic behavior of NO and NO_2 on the surfaces of GaP nanosheet (Table 4). "μ" which shows chemical potential accompanying negative worth using B3LYP/ LANL2DZ, 6-311+G (d, p), has an agreeable yield for capturing NO and NO_2 by GaP nanosheet (Table 4).

The illustration of donor-acceptor molecules depends on the relative frontier molecular levels. The HOMO-LUMO gap defines the charge transfer in gas molecules adsorbed on the GaP surface through the simplified molecular-level diagram. In fact, the number of transferred charges might be considerably small, as in the case of parallel and perpendicular coordination, which indicates electronic couplings are smaller than in co-facial coordination. The results in Table 4 have indicated the energy level shifts of gas molecule →surface-HOMO and gas molecule → surface-LUMO of nanoclusters as a function of their distance *d* orbitals from the high symmetry points of each gas

molecule on the GaP surface. Therefore, the HOMO level of the molecule is lowered as it loses its electron, whereas the LUMO level of the surface is raised as it gains partial charge.

4. Conclusions

This research aimed to illustrate gas adsorption on GaP nanosheets. The structural, energetic, and infrared adsorption properties of linearly "atop" for NO and NO_2 molecules adsorbing on GaP nanosheet have been explored using DFT calculations.

The values of charge density changes have shown a more important charge transfer for GaP, which acts as the electron acceptor and gas molecules and the stronger electron donor through adsorption on the graphitic-like GaP surface. It has been assumed that the priority for selecting the surface binding of N-atom of NO and O-atom of NO_2 in the adsorption site can be impacted by the existence of close atoms in the GaP surface.

Finally, our molecular simulation consequences have exhibited the existence of orbital hybridization between gallium sites and gas molecules of NO and NO_2, which also approves the recovery of adsorption susceptibility of graphene sheets. In fact, the GaP nanosheet can promise an applicable outlook in the NO and NO2 gas sensor field.

Funding

This research received no external funding.

Acknowledgments

In successfully completing this paper and its research, the authors are grateful to Kastamonu University.

Conflicts of Interest

The authors declare no conflict of interest.

References

1. Liao, Y.; Peng, R.; Peng, S.; Zeng, W.; Zhou, Q. The Adsorption of H_2 and C_2H_2 on Ge-Doped and Cr-Doped Graphene Structures: A DFT Study. *Nanomaterials* **2021**, *11*, 231, https://doi.org/10.3390/nano11010231.
2. Monajjemi, M.; Jafari Azan, M.; Mollaamin, F. Density functional theory study on B30N20 nanocage in structural properties and thermochemical outlook. *Fullerenes Nanotubes and Carbon Nanostructures* **2013**, *21*, 503-515, https://doi.org/10.1080/1536383X.2011.629762.
3. Costa, M.C.F.; Marangoni, V.S.; Ng, P.R.; Nguyen, H.T.L.; Carvalho, A.; Castro Neto, A.H. Accelerated Synthesis of Graphene Oxide from Graphene. *Nanomaterials* **2021**, *11*, 551, https://doi.org/10.3390/nano11020551.
4. Tahan, A.; Mollaamin, F.; Monajjemi, M. Thermochemistry and NBO analysis of peptide bond: Investigation of basis sets and binding energy. *Russian Journal of Physical Chemistry A* **2009**, *83*, 587-597, https://doi.org/10.1134/S003602440904013X.
5. Zadeh, M.A.A.; Lari, H.; Kharghanian, L.; Balali, E.; Khadivi, R.; Yahyaei, H.; Mollaamin, F.; Monajjemi, M. Density functional theory study and anti-cancer properties of shyshaq plant: In view point of nano biotechnology, *J. Comput. Theor. Nanosci* **2015**, *12*, 4358-4367, https://doi.org/10.1166/jctn.2015.4366.
6. Mollaamin, F.; Monajjemi, M. Harmonic Linear Combination and Normal Mode Analysis of Semiconductor Nanotubes Vibrations. *J. Comput. Theor. Nanosci* **2015**, *12*, 1030-1039, https://doi.org/10.1166/jctn.2015.3846.

7. Bekeschus, S. Combined Toxicity of Gas Plasma Treatment and Nanoparticles Exposure in Melanoma Cells In Vitro. *Nanomaterials* **2021**, *11*, 806, https://doi.org/10.3390/nano11030806.
8. Xiong, H.H.; Zhang, H.H.; Gan, L. A new bifunctional C3N nanosheet of NO2, SO2 gas sensor and CO2 separation: A first-principles study. *Phys. E* **2021**, *126*, 114463, https://doi.org/10.1016/j.physe.2020.114463.
9. Mollaamin, F.; Monajjemi, M. Tailoring and functionalizing the graphitic-like GaN and GaP nanostructures as selective sensors for NO, NO2, and NH3 adsorbing: a DFT study. *J Mol Model* **2023**, *29*, 170. https://doi.org/10.1007/s00894-023-05567-8.
10. Monajjemi, M.; Baheri, H.; Mollaamin, F. A percolation model for carbon nanotube-polymer composites using the Mandelbrot-Given. *Journal of Structural Chemistry* **2011**, *52*, 54-59, https://doi.org/10.1134/S0022476611010070.
11. Liao, Y.M.; Peng, R.C.; Peng, S.D.; Zeng, W.; Zhou, Q. The adsorption of H2 and C2H2 on Ge-doped and Cr-doped graphene structures: A DFT study. *Nanomaterial* **2021**, *11*, 231, https://doi.org/10.3390/nano11010231.
12. Gao, X.; Zhou, Q.; Wang, J.X.; Xu, L.N.; Zeng, W. DFT Study on the Selective Adsorption Properties of Modified Graphene for SF6 Decompositions. *IEEE Sens. J.* **2021**, *21*, 3193–3200, https://doi.org/10.1109/JSEN.2020.3027359.
13. Monajjemi, M.; Najafpour, J.; Mollaamin, F. $(3,3)_4$ Armchair carbon nanotube in connection with PNP and NPN junctions: Ab Initio and DFT-based studies. *Fullerenes Nanotubes and Carbon Nanostructures* **2013**, *21*, 213-232, https://doi.org/10.1080/1536383X.2011.597010.
14. Yang, S.; Lei, G.; Xu, H.; Lan, Z.; Wang, Z.; Gu, H. Metal Oxide Based Heterojunctions for Gas Sensors: A Review. *Nanomaterials* **2021**, *11*, 1026, https://doi.org/10.3390/nano11041026.
15. Keloth Paduvilan, J.; Velayudhan, P.; Amanulla, A.; Joseph Maria, H.; Saiter-Fourcin, A.; Thomas, S. Assessment of Graphene Oxide and Nanoclay Based Hybrid Filler in Chlorobutyl-Natural Rubber Blend for Advanced Gas Barrier Applications. *Nanomaterials* **2021**, *11*, 1098, https://doi.org/10.3390/nano11051098.
16. Prekob, Á.; Udayakumar, M.; Karacs, G.; Kristály, F.; Muránszky, G.; Leskó, A.K.; Németh, Z.; Viskolcz, B.; Vanyorek, L. Development of Highly Efficient, Glassy Carbon Foam Supported, Palladium Catalysts for Hydrogenation of Nitrobenzene. *Nanomaterials* **2021**, *11*, 1172, https://doi.org/10.3390/nano11051172.
17. Mahdavian, L.; Monajjemi, M. Alcohol sensors based on SWNT as chemical sensors: Monte Carlo and Langevin dynamics simulation. *Microelectronics journal* **2010**, *41*, 142-149, https://doi.org/10.1016/j.mejo.2010.01.011.
18. Han, T.-H.; Bak, S.-Y.; Kim, S.; Lee, S.H.; Han, Y.-J.; Yi, M. Decoration of CuO NWs Gas Sensor with ZnO NPs for Improving NO_2 Sensing Characteristics. *Sensors* **2021**, *21*, 2103, https://doi.org/10.3390/s21062103.
19. Monajjemi, M.; Mahdavian, L.; Mollaamin, F.; Khaleghian, M. Interaction of Na, Mg, Al, Si with carbon nanotube (CNT): NMR and IR study. *Russ. J. Inorg. Chem* **2009**, *54*, 1465-1473, https://doi.org/10.1134/S0036023609090216.
20. Tonezzer, M.; Thai, N.X.; Gasperi, F.; Van Duy, N.; Biasioli, F. Quantitative Assessment of Trout Fish Spoilage with a Single Nanowire Gas Sensor in a Thermal Gradient. *Nanomaterials* **2021**, *11*, 1604, https://doi.org/10.3390/nano11061604.
21. Mollaamin, F.; Ilkhani, A.; Sakhaei, N.; Bonsakhteh, B.; Faridchehr, A.; Tohidi, S.; Monajjemi, M. Thermodynamic and solvent effect on dynamic structures of nano bilayer-cell membrane: Hydrogen bonding study. *Journal of Computational and Theoretical Nanoscience* **2015**, *12*, 3148-3154, https://doi.org/10.1166/jctn.2015.4092.
22. Chang, H.-K.; Ko, D.-S.; Cho, D.-H.; Kim, S.; Lee, H.-N.; Lee, H.S.; Kim, H.-J.; Park, T.J.; Park, Y.M. Enhanced response of the photoactive gas sensor on formaldehyde using porous SnO2@TiO2 heterostructure driven by gas-flow thermal evaporation and atomic layer deposition. *Ceram. Int.* **2021**, *47*, 5985–5992, https://doi.org/10.1016/j.ceramint.2020.10.172.

23. Monajjemi, M.; Khaleghian, M.; Tadayonpour, N.; Mollaamin, F. The effect of different solvents and temperatures on stability of single-walled carbon nanotube: A QM/MD study. *Int. J. Nanosci.* **2010**, *09*, 517-529, https://doi.org/10.1142/S0219581X10007071.
24. Khalili Hadad, B., Mollaamin, F., Monajjemi, M. Biophysical chemistry of macrocycles for drug delivery: A theoretical study. *Russian Chemical Bulletin*, **2011**,*60*, 238-241, https://doi.org/10.1007/s11172-011-0039-5.
25. Huang, J.; Jiang, D.; Zhou, J.; Ye, J.; Sun, Y.; Li, X.; Geng, Y.; Wang, J.; Du, Y.; Qian, Z. Visible light-activated room temperature NH3 sensor base on CuPc-loaded ZnO nanorods. *Sens. Actuators B Chem.* **2021**, *327*, 128911, https://doi.org/10.1016/j.snb.2020.128911.
26. Tonezzer, M. Detection of mackerel fish spoilage with a gas sensor based on one single SnO2 nanowire. *Chemosensors* **2021**, *9*, 1–10, https://doi.org/10.3390/chemosensors9010002.
27. Ding, Y.; Guo, X.; Du, B.; Hu, X.; Yang, X.; He, Y.; Zhou, Y.; Zang, Z. Low-operating temperature ammonia sensor based on Cu_2O nanoparticles decorated with p-type MoS_2 nanosheets. *J. Mater. Chem. C* **2021**, *9*, 4838–4846, https://doi.org/10.1039/D1TC00391G.
28. Zhang, J.; Leng, D.; Zhang, L.; Li, G.; Ma, F.; Gao, J.; Lu, H.; Zhu, B. Porosity and oxygen vacancy engineering of mesoporous WO3 nanofibers for fast and sensitive low-temperature NO2 sensing. *J. Alloys Compd.* **2021**, *853*, 157339, https://doi.org/10.1016/j.jallcom.2020.157339.
29. Shahriari, S.; Mollaamin, F.; Monajjemi, M. Increasing the Performance of {[(1-x-y) LiCo0.3Cu0.7] (Al and Mg doped)] O2}, xLi2MnO3, yLiCoO2 Composites as Cathode Material in Lithium-Ion Battery: Synthesis and Characterization. *Micromachines* **2023**, *14*, 241. https://doi.org/10.3390/mi14020241.
30. Mollaamin, F.; Monajjemi, M. In Silico-DFT Investigation of Nanocluster Alloys of Al-(Mg, Ge, Sn) Coated by Nitrogen Heterocyclic Carbenes as Corrosion Inhibitors. *J Clust Sci* **2023**, *34*, 2901–2918. https://doi.org/10.1007/s10876-023-02436-5.
31. Monajjemi, M.; Mollaamin,F.; Shojaei, S. An overview on Coronaviruses family from past to Covid-19: Introduce some inhibitors as antiviruses from Gillan's plants. *Biointerface Res. Appl. Chem.* **2020**, *10*, 5575 . doi:org/10.33263/BRIAC103.575585.
32. Thi Dang, D.M.; Monajjemi, M.; Mollaamin, F.; Dang, C.M. Molecular Dynamics Simulation from Symmetry Breaking Changing to Asymmetrical Phospholipid Membranes Due to Variable Capacitors during Resonance with Helical Proteins. *Symmetry* **2023**, *15*, 1259. https://doi.org/10.3390/sym15061259.
33. 33.Sarasia, E.M.; Afsharnezhad, S.; Honarparvar, B.; Mollaamin, F.; Monajjemi, M. Theoretical study of solvent effect on NMR shielding tensors of luciferin derivatives. *Phys Chem Liquids* **2011**, *49*, 561-571, https://doi.org/10.1080/00319101003698992.
34. Ghalandari, B.; Monajjemi, M.; Mollaamin, F. Theoretical Investigation of Carbon Nanotube Binding to DNA in View of Drug Delivery. *J.Comput.Theor.Nanosci* **2011**, *8*, 1212-1219, https://doi.org/10.1166/jctn.2011.1801.
35. Alharbi, A.; Junker, B.; Alduraibi, M.; Algarni, A.; Weimar, U.; Bârsan, N. The Role of Different Lanthanoid and Transition Metals in Perovskite Gas Sensors. *Sensors* **2021**, *21*, 8462, https://doi.org/10.3390/s21248462.
36. Andreev, M.; Platonov, V.; Filatova, D.; Galitskaya, E.; Polomoshnov, S.; Generalov, S.; Nikolaeva, A.; Amelichev, V.; Zhdaneev, O.; Krivetskiy, V.; Rumyantseva, M. Flame-Made La_2O_3-Based Nanocomposite CO_2 Sensors as Perspective Part of GHG Monitoring System. *Sensors* **2021**, *21*, 7297, https://doi.org/10.3390/s21217297.
37. Ahn, J.; Kim, D.; Park, K.-H.; Yoo, G.; Heo, J. Pt-Decorated Graphene Gate AlGaN/GaN MIS-HEMT for Ultrahigh Sensitive Hydrogen Gas Detection. IEEE Trans. *Electron. Devices* **2021**, *68*, 1255–1261, https://doi.org/10.1109/TED.2021.3053515.

38. Vuong, T.-A.; Cha, H.-Y.; Kim, H. Response Enhancement of Pt–AlGaN/GaN HEMT Gas Sensors by Thin AlGaN Barrier with the Source-Connected Gate Configuration at High Temperature. *Micromachines* **2021**, *12*, 537, https://doi.org/10.3390/mi12050537.
39. Nguyen, V.C.; Kim, K.; Kim, H. Performance Optimization of Nitrogen Dioxide Gas Sensor Based on Pd-AlGaN/GaN HEMTs by Gate Bias Modulation. *Micromachines* **2021**, *12*, 400, https://doi.org/10.3390/mi12040400.
40. Geng, X.; Liu, X.; Mawella-Vithanage, L.; Hewa-Rahinduwage, C.C.; Zhang, L.; Brock, S.L.; Tan, T.; Luo, L. Photoexcited NO_2 Enables Accelerated Response and Recovery Kinetics in Light-Activated NO_2 Gas Sensing. *ACS Sens.* **2021**, *6*, 4389–4397, https://doi.org/10.1021/acssensors.1c01694.
41. Šetka, M.; Claros, M.; Chmela, O.; Vallejos, S. Photoactivated Materials and Sensors for NO_2 Monitoring. *J. Mater. Chem. C* **2021**, *9*, 16804–16827, https://doi.org/10.1039/D1TC04247E.
42. Reddeppa, M.; KimPhung, N.T.; Murali, G.; Pasupuleti, K.S.; Park, B.-G.; In, I.; Kim, M.-D. Interaction Activated Interfacial Charge Transfer in 2D G-C3N4/GaN Nanorods Heterostructure for Self-Powered UV Photodetector and Room Temperature NO_2 Gas Sensor at ppb Level. *Sens. Actuators B Chem.* **2021**, *329*, 129175, https://doi.org/10.1016/j.snb.2020.129175.
43. Shin, J.; Han, S.; Noh, S.; Yu, Y.-T.; Kim, J.S. Room-Temperature Operation of Light-Assisted NO2 Gas Sensor Based on GaN Nanowires and Graphene. *Nanotechnology* **2021**, *32*, 505201, https://doi.org/10.1088/1361-6528/ac2427.
44. Hwang, J.; Jung, H.; Shin, H.-S.; Kim, D.-S.; Kim, D.S.; Ju, B.-K.; Chun, M. The Effect of Noble Metals on CO Gas Sensing Properties of In2O3 Nanoparticles. *Appl. Sci.* **2021**, *11*, 4903, https://doi.org/10.3390/app11114903.
45. Hou, X.; Zou, Y.; Ding, M.; Qin, Y.; Zhang, Z.; Ma, X.; Tan, P.; Yu, S.; Zhou, X.; Zhao, X.; et al. Review of polymorphous Ga2O3 materials and their solar-blind photodetector applications. *J. Phys. D Appl. Phys.* **2021**, *54*, 043001, https://doi.org/10.1088/1361-6463/abbb45.
46. Tak, B.R.; Kumar, S.; Kapoor, A.K.; Wang, D.; Li, X.; Sun, H.; Singh, R. Recent advances in the growth of gallium oxide thin films employing various growth techniques—A review. *J. Phys. D Appl. Phys.* **2021**, *54*, 453002, https://doi.org/10.1088/1361-6463/ac1af2.
47. Blevins, J.; Yang, G. On optical properties and scintillation performance of emerging Ga2O3: Crystal growth, emission mechanisms and doping strategies. *Mater. Res. Bull.* **2021**, *144*, 111494, https://doi.org/10.1016/j.materresbull.2021.111494.
48. Yuan, Y.; Hao, W.; Mu, W.; Wang, Z.; Chen, X.; Liu, Q.; Xu, G.; Wang, C.; Zhou, H.; Zou, Y.; et al. Toward emerging gallium oxide semiconductors: A roadmap. *Fundam. Res.* **2021**, *1*, 697–716, https://doi.org/10.1016/j.fmre.2021.11.002.
49. Huang, H.-C.; Ren, Z.; Chan, C.; Li, X. Wet etch, dry etch, and MacEtch of β-Ga2O3: A review of characteristics and mechanism. *J. Mater. Res.* **2021**, *36*, 4756–4770, https://doi.org/10.1557/s43578-021-00413-0.
50. Mollaamin, F.; Monajjemi, M. Transition metal (X = Mn, Fe, Co, Ni, Cu, Zn)-doped graphene as gas sensor for CO_2 and NO_2 detection: a molecular modeling framework by DFT perspective. *J Mol Model* **2023**, *29*, 119, https://doi.org/10.1007/s00894-023-05526-3.
51. Mollaamin, F.; Monajjemi, M. Graphene Embedded with Transition Metals for Capturing Carbon Dioxide: Gas Detection Study Using QM Methods. *Clean Technol.* **2023**, *5*, 403–417, https://doi.org/10.3390/cleantechnol5010020.
52. Galazka, Z.; Ganschow, S.; Irmscher, K.; Klimm, D.; Albrecht, M.; Schewski, R.; Pietsch, M.; Schulz, T.; Dittmar, A.; Kwasniewski, A.; et al. Bulk single crystals of β-Ga2O3 and Ga-based spinels as ultra-wide bandgap transparent semiconducting oxides. Prog. Cryst. Growth Charact. *Mater.* **2021**, *67*, 100511, https://doi.org/10.1016/j.pcrysgrow.2020.100511.

53. Sharma, R.; Law, M.E.; Ren, F.; Polyakov, A.Y.; Pearton, S.J. Diffusion of dopants and impurities in β-Ga2O3. *J. Vac. Sci. Technol. A* **2021**, *39*, 060801, https://doi.org/10.1116/6.0001307.
54. Lv, J.; Zhang, H.; Liu, C.; Yi, Z.; Wang, F.; Mu, H.; Li, X.; Sun, T.; Chu, P.K. Optical Anapole Modes in Gallium Phosphide Nanodisk with Forked Slits for Electric Field Enhancement. *Nanomaterials* **2021**, *11*, 1490, https://doi.org/10.3390/nano11061490.
55. Monajjemi, M.; Mollaamin, F.; Gholami, M.R.; Yoosbashizadeh, H.; Sadrnezhad, S.K.; Passdar, H. Quantum Chemical Parameters of Some Organic Corrosion Inhibitors, Pyridine, 2-Picoline 4-Picoline and 2,4-Lutidine, Adsorption at Aluminum Surface in Hydrochloric and Nitric Acids and Comparison Between Two Acidic Media. *Main Group Met. Chem.* **2003**, *26*, 349-362, https://doi.org/10.1515/MGMC.2003.26.6.349.
56. Papež, N.; Dallaev, R.; Ţălu, Ş.; Kaštyl, J. Overview of the Current State of Gallium Arsenide-Based Solar Cells. *Materials* **2021**, *14*, 3075, https://doi.org/10.3390/ma14113075.
57. Peng, R.; Zhou, Q.; Zeng, W. First-Principles Insight into Pd-Doped C_3N Monolayer as a Promising Scavenger for NO, NO_2 and SO_2. *Nanomaterials* **2021**, *11*, 1267. https://doi.org/10.3390/nano11051267.
58. Mollaamin, F. & Monajjemi, M. Molecular modelling framework of metal-organic clusters for conserving surfaces: Langmuir sorption through the TD-DFT/ONIOM approach. *Molecular Simulation* **2023**, *49*, 365-376, https://doi.org/10.1080/08927022.2022.2159996.
59. Yan, Z.Q.; Tao, C.; Bai, Y.; Liu, S.P. Adsorption of nitrogen based gas molecules on noble metal functionalized carbon nitride nanosheets: A theoretical investigation. *Comput. Theor. Chem.* **2021**, *1194*, 112950, https://doi.org/10.1016/j.comptc.2020.112950.
60. Li, J.; Aierken, A.; Zhuang, Y.; Xu, P.Q.; Wu, H.Q.; Zhang, Q.Y.; Wang, X.B.; Mo, J.H.; Yang, X.; Chen, Q.Y.; et al. 1 MeV electron and 10 MeV proton irradiation effects on inverted metamorphic GaInP/GaAs/InGaAs triple junction solar cell. *Sol. Energy Mater. Sol. Cells* **2021**, *224*, 111022, https://doi.org/10.1016/j.solmat.2021.111022.
61. Pinder RW, Walker JT, Bash JO, Cady-Pereira KE, Henze DK, Luo M, et al. Quantifying spatial and temporal variability in atmospheric ammonia with in situ and space-based observations. *Geophys Res Lett.* **2011**, *38*,:L04 802, https://doi.org/10.1029/2010GL046146.
62. Langridge JM, Lack D, Brock CA, Bahreini R, Middlebrook AM, Neuman JA, et al. Evolution of aerosol properties impacting visibility and direct climate forcing in an ammonia-rich urban environment. *J Geophys Res-Atmos* **2012**, *117*, D00v11, https://doi.org/10.1029/2011jd017116.
63. Gruginskie, N.; Cappelluti, F.; van Eerden, M.; Bauhuis, G.; Mulder, P.; Vlieg, E.; Schermer, J. Proton irradiation induced GaAs solar cell performance degradation simulations using a physics-based model. *Sol. Energy Mater. Sol. Cells* **2021**, *223*, 110971, https://doi.org/10.1016/j.solmat.2021.110971.
64. Kondratev,V.M.; Kuznetsov,A.; Fedina, S.V.; Nalimova,S.S.; Moshnikov, V.A. and Bolshakov, A.D. Gallium phosphide nanowires for "biological concentrations" ammonia detection. *J. Phys.: Conf. Ser.* **2022**, *2172*, 012006, https://doi.org/10.1088/1742-6596/2172/1/012006.
65. Kim, T.; Lee, S.; Cho, W.; Kwon, Y.M.; Baik, J.M.; Shin, H. Development of a Novel Gas-Sensing Platform Based on a Network of Metal Oxide Nanowire Junctions Formed on a Suspended Carbon Nanomesh Backbone. *Sensors* **2021**, *21*, 4525, https://doi.org/10.3390/s21134525.
66. Mollaamin, F.; Monajjemi, M. Trapping of toxic heavy metals from water by GN–nanocage: Application of nanomaterials for contaminant removal technique. *J. Mol. Struct* **2024**, *1300*, 137214. https://doi.org/10.1016/j.molstruc.2023.137214.
67. Frisch, M. J.; Trucks, G. W.; Schlegel, H. B.; Scuseria, G. E.; Robb, M. A.; Cheeseman, J. R.; Scalmani, G.; Barone, V.; Petersson, G. A.; Nakatsuji, H. et al. Gaussian 16, Revision C.01, Gaussian, Inc., Wallingford CT, **2016**, https://gaussian.com/citation/.

68. Singh, A.K.; Zhuang, H. L. and Hennig, R. G. Ab initio synthesis of single-layer III-V materials. Phys. Rev. B: Condens. *Matter Mater. Phys.* **2014**, *89*, 245431, https://doi.org/10.1103/PhysRevB.89.245431.
69. Mollaamin, F.; Monajjemi, M. Corrosion Inhibiting by Some Organic Heterocyclic Inhibitors Through Langmuir Adsorption Mechanism on the Al-X (X = Mg/Ga/Si) Alloy Surface: A Study of Quantum Three-Layer Method of CAM-DFT/ONIOM. *J Bio Tribo Corros* **2023**, *9*, 33, https://doi.org/10.1007/s40735-023-00751-y.
70. Mollaamin, F.; Shahriari, S.; Monajjemi, M. et al. Nanocluster of Aluminum Lattice via Organic Inhibitors Coating: A Study of Freundlich Adsorption. *J Clust Sci* **2023**, *34*, 1547–1562. https://doi.org/10.1007/s10876-022-02335-1.
71. Mollaamin, F.; Monajjemi, M. Doping of Graphene Nanostructure with Iron, Nickel and Zinc as Selective Detector for the Toxic Gas Removal: A Density Functional Theory Study. *C-Journal of Carbon Research* **2023**, *9*, 20, https://doi.org/10.3390/c9010020.
72. Perdew, J.P.; Burke, K.; Ernzerhof, M. Generalized Gradient Approximation Made Simple. *Phys. Rev. Lett.* **1996**, *77*, 3865-3868, https://doi.org/10.1103/PhysRevLett.77.3865.
73. Mollaamin, F.; Monajjemi, M.; Salemi, S.; Baei, M.T. A Dielectric Effect on Normal Mode Analysis and Symmetry of BNNT Nanotube. *Fuller. Nanotub. Carbon Nanostructures* **2011**, *19*, 182-196, https://doi.org/10.1080/15363831003782932.
74. Monajjemi, M.; Noei M.; Mollaamin,F. *Nucleos. Nucleot. Nucl.* **2010**, *29*, 676–683. https://doi.org/10.1080/15257771003781642.
75. Xie, C.; Sun, Y.; Zhu, B.; Song, W.; Xu, M. Adsorption mechanism of NH_3, NO, and O_2 molecules over the FexOy/AC catalyst surface: A DFT-D3 study. *New J. Chem.* **2021**, *45*, 3169–3180, https://doi.org/10.1039/D0NJ05628F.
76. Monajjemi, M.; Mollaamin, F.; Gholami, M. R. et al., Quantum Chemical Parameters of Some Organic Corrosion Inhibitors, Pyridine, 2-Picoline 4-Picoline and 2,4-Lutidine, Adsorption at Aluminum Surface in Hydrocholoric and Nitric Acids and Comparison Between Two Acidic Media. *Main Group Met. Chem.* **2003**, *26*, 349 . https://doi.org/10.1515/MGMC.2003.26.6.349
77. Mollaamin, F. and Monajjemi, M. Graphene-based resistant sensor decorated with Mn, Co, Cu for nitric oxide detection: Langmuir adsorption & DFT method, *Sensor Review*, **2023**, *43*, 266-279. https://doi.org/10.1108/SR-03-2023-0040.
78. Bakhshi, K.; Mollaamin, F.; Monajjemi, M. Exchange and correlation effect of hydrogen chemisorption on nano V(100) surface: A DFT study by generalized gradient approximation (GGA). *J.Comput.Theor.Nanosci*, **2011**, *8*,763-768, https://doi.org/10.1166/jctn.2011.1750.
79. Khaleghian, M.; Zahmatkesh, M.; Mollaamin, F. et al., Investigation of Solvent Effects on Armchair Single-Walled Carbon Nanotubes: A QM/MD Study. *Fuller. Nanotub. Carbon Nanostruct*. **2011**, *19*, 251–261. https://doi.org/10.1080/15363831003721757.
80. Mollaamin, F.; Monajjemi, M. Electric and Magnetic Evaluation of Aluminum–Magnesium Nanoalloy Decorated with Germanium Through Heterocyclic Carbenes Adsorption: A Density Functional Theory Study. *Russ. J. Phys. Chem. B* **2023**, *17*, 658–672. https://doi.org/10.1134/S1990793123030223.
81. Monajjemi, M.; Baie, M.T.; Mollaamin, F. Interaction between threonine and cadmium cation in [Cd(Thr)] (n = 1-3) complexes: Density functional calculations. *Russian Chemical Bulletin*, **2010**, *59*, 886-889, https://doi.org/10.1007/s11172-010-0181-5.
82. Svensson,M.; Humbel,S.; Froese,R.D.J.; Matsubara,T.; Sieber,S.; and Morokuma,K. ONIOM: A Multilayered Integrated MO + MM Method for Geometry Optimizations and Single Point Energy Predictions. A Test for Diels−Alder Reactions and Pt(P(t-Bu)3)2 + H2 Oxidative Addition. *J. Phys. Chem.* **1996**, *100*, 19357–19363, https://doi.org/10.1021/jp962071j.

83. Takeshi Yanai , David P Tew , Nicholas C Handy. A new hybrid exchange–correlation functional using the Coulomb-attenuating method (CAM-B3LYP). *Chemical Physics Letters*, **2004**, *393*, 51-57, https://doi.org/10.1016/j.cplett.2004.06.011.
84. Lehtola, S. A review on non-relativistic fully numerical electronic structure calculations on atoms and diatomic molecules. *Int. J. Quantum Chem*. **2019**, *119*, https://doi.org/10.1002/qua.25968.
85. Mollaamin, F. Computational Methods in the Drug Delivery of Carbon Nanocarriers onto Several Compounds in Sarraceniaceae Medicinal Plant as Monkeypox Therapy. Computation 2023, 11, 84. https://doi.org/10.3390/computation11040084.
86. Monajjemi, M.; Honaparvar, B.; Khalili Hadad, B.; Ilkhani, A.; Mollaamin, F. Thermo-Chemical Investigation and NBO Analysis of Some anxileotic as Nano- Drugs. *African journal of pharmacy and pharmacology* **2010**, *4*, 521-529, https://www.researchgate.net/publication/304742272.
87. Hartman, J.D.; Mathews, A. and Harper, J.K. Fast and Accurate Electric Field Gradient Calculations in Molecular Solids With Density Functional Theory. *Front. Chem., Sec. Theoretical and Computational Chemistry* **2021**, *9*, 751711, https://doi.org/10.3389/fchem.2021.751711.
88. Young, H.A.; Freedman, R. D. *Sears and Zemansky's University Physics with Modern Physics* (13th ed.). Boston: Addison-Wesley. **2012**, 754, https://www.amazon.com/Sears-Zemanskys-University-Physics-Modern/dp/0321696867.
89. Monajjemi, M.; Farahani, N.; & . Mollaamin, F. Thermodynamic study of solvent effects on nanostructures: phosphatidylserine and phosphatidylinositol membranes. *Phys. Chem. Liq*. **2012**, *50*, 161-172. https://doi.org/10.1080/00319104.2010.527842.
90. Kohn, W.; Becke, A.D.; Parr, R.G. Density Functional Theory of Electronic Structure. *J. Phys. Chem*. **1996**, *100*, 12974–12980, https://doi.org/10.1021/jp960669l.
91. Parr, R.G. and Pearson, R.G. (1983) Absolute Hardness: Companion Parameter to Absolute Electronegativity. *J. Am. Chem. Soc.* **1983**, *105*, 7512-7516, http://dx.doi.org/10.1021/ja00364a005.
92. Monajjemi,M.; Lee, V. S.; Khaleghian, M.; Honarparvar,B. and Mollaamin, F. Theoretical Description of Electromagnetic Nonbonded Interactions of Radical, Cationic, and Anionic NH2BHNBHNH2 Inside of the B18N18 Nanoring. *J. Phys. Chem. C* **2010**, *114*, 15315–15330. https://doi.org/10.1021/jp104274z.
93. Mollaamin, F.; Monajjemi, M. Carbon Nanotubes as Biosensors for Releasing Conjugated Bisphosphonates–Metal Ions in Bone Tissue: Targeted Drug Delivery through the DFT Method. *C-Journal of Carbon Research* **2023**, *9*, 61. https://doi.org/10.3390/c9020061.